JOURNAL OF Applied Polymer SCIENCE

Special Issue: Microfiltration and Ultrafiltration Membrane Science and Technology

Guest Editors: Prof. Isabel C. Escobar (University of Toledo) and Prof. Bart Van der Bruggen (University of Leuven)

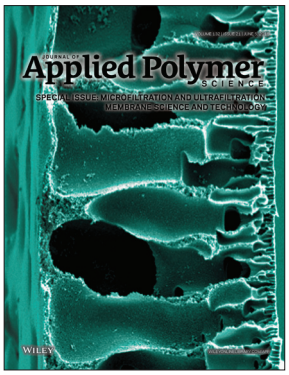

EDITORIAL

Microfiltration and Ultrafiltration Membrane Science and Technology
I. C. Escobar and B. Van der Bruggen, *J. Appl. Polym. Sci.* 2015, **DOI: 10.1002/app.42002**

REVIEWS

Nanoporous membranes generated from self-assembled block polymer precursors: *Quo Vadis*?
Y. Zhang, J. L. Sargent, B. W. Boudouris and W. A. Phillip, *J. Appl. Polym. Sci.* 2015, **DOI: 10.1002/app.41683**

Making polymeric membranes anti-fouling via "grafting from" polymerization of zwitterions
Q. Li, J. Imbrogno, G. Belfort and X.-L. Wang, *J. Appl. Polym. Sci.* 2015, **DOI: 10.1002/app.41781**

Fouling control on MF/ UF membranes: Effect of morphology, hydrophilicity and charge
R. Kumar and A. F. Ismail, *J. Appl. Polym. Sci.* 2015, **DOI: 10.1002/app.42042**

EMERGING MATERIALS AND FABRICATION

Preparation of a poly(phthalazine ether sulfone ketone) membrane with propanedioic acid as an additive and the prediction of its structure
P. Qin, A. Liu and C. Chen, *J. Appl. Polym. Sci.* 2015, **DOI: 10.1002/app.41621**

Preparation and characterization of MOF-PES ultrafiltration membranes
L. Zhai, G. Li, Y. Xu, M. Xiao, S. Wang and Y. Meng, *J. Appl. Polym. Sci.* 2015, **DOI: 10.1002/app.41663**

Tailoring of structures and permeation properties of asymmetric nanocomposite cellulose acetate/silver membranes
A. S. Figueiredo, M. G. Sánchez-Loredo, A. Maurício, M. F. C. Pereira, M. Minhalma and M. N. de Pinho, *J. Appl. Polym. Sci.* 2015, **DOI: 10.1002/app.41796**

LOW-FOULING POLYMERS

Low fouling polysulfone ultrafiltration membrane via click chemistry
Y. Xie, R. Tayouo and S. P. Nunes, *J. Appl. Polym. Sci.* 2015, **DOI: 10.1002/app.41549**

Elucidating membrane surface properties for preventing fouling of bioreactor membranes by surfactin
N. Behary, D. Lecouturier, A. Perwuelz and P. Dhulster, *J. Appl. Polym. Sci.* 2015, **DOI: 10.1002/app.41622**

PVC and PES-*g*-PEGMA blend membranes with improved ultrafiltration performance and fouling resistance
S. Jiang, J. Wang, J. Wu and Y. Chen, *J. Appl. Polym. Sci.* 2015, **DOI: 10.1002/app.41726**

Improved antifouling properties of TiO_2/PVDF nanocomposite membranes in UV coupled ultrafiltration
M. T. Moghadam, G. Lesage, T. Mohammadi, J.-P. Mericq, J. Mendret, M. Heran, C. Faur, S. Brosillon, M. Hemmati and F. Naeimpoor, *J. Appl. Polym. Sci.* 2015, **DOI: 10.1002/app.41731**

Development of functionalized doped carbon nanotube/polysulfone nanofiltration membranes for fouling control
P. Xie, Y. Li and J. Qiu, *J. Appl. Polym. Sci.* 2015, **DOI: 10.1002/app.41835**

JOURNAL OF Applied Polymer SCIENCE

Special Issue: Microfiltration and Ultrafiltration Membrane Science and Technology

Guest Editors: Prof. Isabel C. Escobar (University of Toledo) and
Prof. Bart Van der Bruggen (University of Leuven)

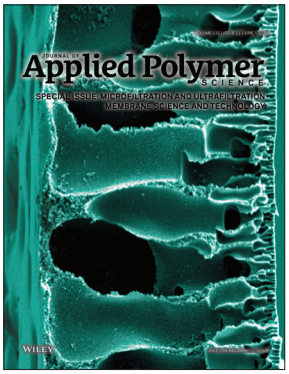

SURFACE MODIFICATION OF POLYMER MEMBRANES

Highly chlorine and oily fouling tolerant membrane surface modifications by *in situ* polymerization of dopamine and poly(ethylene glycol) diacrylate for water treatment
K. Yokwana, N. Gumbi, F. Adams, S. Mhlanga, E. Nxumalo and B. Mamba, *J. Appl. Polym. Sci.* 2015, **DOI: 10.1002/app.41661**

Fouling control through the hydrophilic surface modification of poly(vinylidene fluoride) membranes
H. Jang, D.-H. Song, I.-C. Kim, and Y.-N. Kwon, *J. Appl. Polym. Sci.* 2015, **DOI: 10.1002/app.41712**

Hydroxyl functionalized PVDF-TiO_2 ultrafiltration membrane and its antifouling properties
Y. H. Teow, A. A. Latif, J. K. Lim, H. P. Ngang, L. Y. Susan and B. S. Ooi, *J. Appl. Polym. Sci.* 2015, **DOI: 10.1002/app.41844**

Enhancing the antifouling properties of polysulfone ultrafiltration membranes by the grafting of poly(ethylene glycol) derivatives via surface amidation reactions
H. Yu, Y. Cao, G. Kang, Z. Liu, W. Kuang, J. Liu and M. Zhou, *J. Appl. Polym. Sci.* 2015, **DOI: 10.1002/app.41870**

SEPARATION APPLICATIONS

Experiment and simulation of the simultaneous removal of organic and inorganic contaminants by micellar enhanced ultrafiltration with mixed micelles
A. D. Vibhandik, S. Pawar and K. V. Marathe, *J. Appl. Polym. Sci.* 2015, **DOI: 10.1002/app.41435**

Polymeric membrane modification using SPEEK and bentonite for ultrafiltration of dairy wastewater
A. Pagidi, Y. Lukka Thuyavan, G. Arthanareeswaran, A. F. Ismail, J. Jaafar and D. Paul, *J. Appl. Polym. Sci.* 2015, **DOI: 10.1002/app.41651**

Forensic analysis of degraded polypropylene hollow fibers utilized in microfiltration
X. Lu, P. Shah, S. Maruf, S. Ortiz, T. Hoffard and J. Pellegrino, *J. Appl. Polym. Sci.* 2015, **DOI: 10.1002/app.41553**

A surface-renewal model for constant flux cross-flow microfiltration
S. Jiang and S. G. Chatterjee, *J. Appl. Polym. Sci.* 2015, **DOI: 10.1002/app.41778**

Ultrafiltration of aquatic humic substances through magnetically responsive polysulfone membranes
N. A. Azmi, Q. H. Ng and S. C. Low, *J. Appl. Polym. Sci.* 2015, **DOI: 10.1002/app.41874**

BIOSEPARATIONS APPLICATIONS

Analysis of the effects of electrostatic interactions on protein transport through zwitterionic ultrafiltration membranes using protein charge ladders
M. Hadidi and A. L. Zydney, *J. Appl. Polym. Sci.* 2015, **DOI: 10.1002/app.41540**

Modification of microfiltration membranes by hydrogel impregnation for pDNA purification
P. H. Castilho, T. R. Correia, M. T. Pessoa de Amorim, I. C. Escobar, J. A. Queiroz, I. J. Correia and A. M. Morão, *J. Appl. Polym. Sci.* 2015, **DOI: 10.1002/app.41610**

Hemodialysis membrane surface chemistry as a barrier to lipopolysaccharide transfer
B. Madsen, D. W. Britt, C.-H. Ho, M. Henrie, C. Ford, E. Stroup, B. Maltby, D. Olmstead and M. Andersen, *J. Appl. Polym. Sci.* 2015, **DOI: 10.1002/app.41550**

Membrane adsorbers comprising grafted glycopolymers for targeted lectin binding
H. C. S. Chenette and S. M. Husson, *J. Appl. Polym. Sci.* 2015, **DOI: 10.1002/app.41437**

Journal of Applied Polymer Science

Tailoring of structures and permeation properties of asymmetric nanocomposite cellulose acetate/silver membranes

Ana Sofia Figueiredo,[1,2] María Guadalupe Sánchez-Loredo,[3] António Maurício,[4] Manuel F. C. Pereira,[4] Miguel Minhalma,[1] Maria Norberta de Pinho[2]

[1]Departmental Area of Chemical Engineering, Instituto Superior de Engenharia de Lisboa, Rua Conselheiro Emídio Navarro 1, 1959-007, Lisbon, Portugal

[2]ICEMS/Department of Chemical Engineering, Universidade de Lisboa, Av. Rovisco Pais, 1, 1049-001, Lisbon, Portugal

[3]Instituto de Metalurgia/Facultad de Ingeniería, Universidad Autónoma de San Luis Potosí, Sierra Leona 550, 78210, SLP, México

[4]CEPGIST/CERENA, Instituto Superior Técnico, Universidade de Lisboa, Av. Rovisco Pais, 1, 1049-001, Lisbon, Portugal

Correspondence to: M. G. Sánchez-Loredo (E-mail: msanchez@uaslp.mx)

ABSTRACT: Cellulose acetate (CA)–silver (Ag) nanocomposite asymmetric membranes were prepared via the wet-phase inversion method by dispersing polyvinylpirrolydone-protected Ag nanoparticles in the membrane casting solutions of different compositions. Silver nanoparticles were synthesized *ex situ* and added to the casting solution as a concentrated aqueous colloidal dispersion. The effects of the dispersion addition on the structure and on the selective permeation properties of the membranes were studied by comparing the nanocomposites with the silver-free materials. The casting solution composition played an important role in the adequate dispersion of the silver nanoparticles in the membrane. Incorporation of nanoscale silver and the final silver content resulted in structural changes leading to an increase in the hydraulic permeability and molecular weight cut-off of the nanocomposite membranes.
 J. Appl. Polym. Sci. **2015**, *132*, 41796.

KEYWORDS: composites; membranes; nanoparticles; nanowires and nanocrystals; properties and characterization

Received 27 May 2014; accepted 26 November 2014

DOI: 10.1002/app.41796

INTRODUCTION

Several concepts and systems of nanotechnology are currently being used to enhance the performance of ceramic and polymeric conventional membranes.[1–11] Pendergast and Hoek[11] proposed a semiquantitative ranking of membrane systems based not only on the performance enhancement but also on the commercial readiness.

Despite their large-scale application, pressure-driven membrane processes are still often associated with problems of concentration polarization and membrane fouling. Besides of complying with the important requisite of large-scale manufacturing, the cellulose acetate (CA) membranes prepared by the wet-phase inversion technique offer multiple possibilities of developing novel materials as membrane/nanoparticles composites with lesser tendency to fouling.

Incorporation of nanoparticles during membranes preparation is promising because it allows the design of nanocomposite structures with the desirable structural, mechanical, and separation properties.[5,7] The membranes structure will depend on the physical and chemical properties of the polymer matrix, the casting procedure, type of nanoparticles, and the method used for nanoparticle incorporation. Yu *et al.*[5] prepared silver-loaded cellulose acetate and polyacrylonitrile hollow fibers by the reduction of Ag^+ by *N*,*N*-dimethylformamide, the polymer solvent, with the objective of producing biofouling-resistant ultrafiltration membranes. They found that the skin layer features (porosity, surface porosity, and thickness) and the macrovoid morphology of the support layer are affected by the nanoparticle incorporation. The skin layer determines the permeability, rejection, and selectivity of membranes, and the structure of the support layer its compaction behavior.

The wet-phase inversion process is a simple and versatile technique and allows the tailoring of asymmetric structures of polymeric membranes by the selection of the appropriate casting solutions (polymers, solvent or solvent mixtures, additives), and conditions (evaporation time, coagulation baths) controlling the film forming and the demixing processes.[5,7] De Pinho and coauthors correlated the structural characteristics of

Table I. Casting Solutions Compositions and Film Casting Conditions of the CA400 Series Membranes Free of Silver and with Silver Nanoparticles

Membrane	CA400-22	CA400-22Ag0.1	CA400-30	CA400-30Ag0.1	CA400-30Ag0.4	CA400-34	CA400-34Ag0.1
Casting solution (wt %)							
Cellulose acetate	17.0	16.4	17.0	16.4	15.2	17.0	16.4
Formamide	22.0	21.2	30.0	29.0	26.9	34.0	32.8
Acetone	61.0	58.9	53.0	51.1	47.5	49.0	47.3
Silver nanoparticles							
Dispersion	-	3.4	-	3.4	10.0	-	3.4
Silver	-	0.1	-	0.1	0.4	-	0.1

Casting conditions		
Temperature of solution (°C)	-	20–25
Temperature of atmosphere (°C)	-	20–25
Solvent evaporation time (min)	-	0.5
Gelation medium	-	Ice-cold water (1–2 h)

cellulose acetate (CA) membrane prepared by the wet-phase inversion method with selective transport properties and the parameters pertaining to different casting solutions and conditions with the membrane structures and the selective transport properties.[12–15]

Abedini *et al.*[16] reported that the addition of hydrophilic TiO_2 nanoparticles promoted formation of macrovoids and more porous structures. They suggested that the rate of demixing during the film casting affects the membranes morphology. Instantaneous demixing often leads to the formation of macrovoids in membrane structure, whereas slow demixing results in denser structures. Hachisuka *et al.* stated that the volatility of the cosolvent has a strong effect on obtaining thinner skin layers and sublayers. This effect possibly depends on the exchange rate between cosolvent and nonsolvent.[17]

The present work addresses an ensemble of parameters for the preparation of cellulose acetate (CA) –silver nanocomposite asymmetric membranes, for example, casting composition, pore former additives, and silver nanoparticles incorporation and its influence on the enhancement of membrane-selective permeation performance with view to obtain membranes with biofouling control and bactericide properties. Special attention is given to a new method of incorporation of concentrated aqueous solutions of nanoparticles with the control of nonagglomeration in the casting formulations to obtain well-dispersed Ag distributions on the membrane polymeric matrices, which is of crucial importance to define the membranes bactericide properties. The polyvinylpyrrolidone-coated Ag nanoparticles were synthetized *ex situ* and added to the casting solutions, where the ratios of CA/acetone/formamide varied from 17 : 61 : 22, 17 : 53 : 30 to 17 : 49 : 34. The silver aqueous dispersions were added to the casting solutions to obtain a final content of 0.1 and 0.4 mass % in silver. The effects of the nanoparticles dispersion and casting solutions composition on the membrane structures were investigated by field emission scanning electron microscopy (FESEM) and microcomputerized tomography (microCT). In order to have a better understanding on the effect of the dispersion addition, pristine cellulose acetate CA-400 membranes were also prepared and characterized. Permeation characteristics of the nanocomposite membranes were compared with the ones of pristine silver-free membrane counterparts.

EXPERIMENTAL

According to the specific needs for the membrane casting solutions, the nanoparticle synthesis protocol of Tashdjian *et al.*[18] was modified with the aim of obtaining a concentrated nanoparticle aqueous dispersion. The preparation was carried out by a dropwise addition of 2 mL of the borohydride solution (1 $molL^{-1}$ $NaBH_4$) to 2 mL of the metal ion solution (0.72 M $AgNO_3$ in water). Both solutions contained 0.02 g of PVPmL^{-1}, and the precipitation was carried out under sonication. The obtained nanoparticles dispersion had a caramel color tone and a homogeneous appearance. To detect the surface plasmon resonance band characteristic of silver nanoparticles, UV/VIS spectroscopy was used. The PVP-coated Ag nanoparticles dispersion presents a peak in the absorption spectra at 406 nm, which is within the range of typical absorption band of Ag nanoparticles (350 nm to 450 nm) and indicating the presence of spherical nanoparticles. According to Desai *et al.*,[19] the presence of nanoparticles agglomerates is characterized by the emergence of a peak above the 600 nm. To evaluate the agglomeration of nanoparticles in the dope solution, the absorbance of casting solution with the Ag nanoparticles was also measured. For casting solutions CA400-30Ag0.1 and CA400-30Ag0.4, a peak was revealed at 444 nm and 452 nm, respectively, giving clear evidence of the absence of nanoparticles aggregation. The nanoparticles dispersion prepared in this work revealed to be stable more than 6 months, maintaining the caramel color tone and the homogeneous appearance. With respect to the absorption peak, the surface plasmon resonance revealed a red-shift to 412 nm, still in the range of spherical nanoparticles.

CA and CA/Ag flat sheet membranes were prepared by the wet-phase inversion method described by Kunst and Sourirajan.[20]

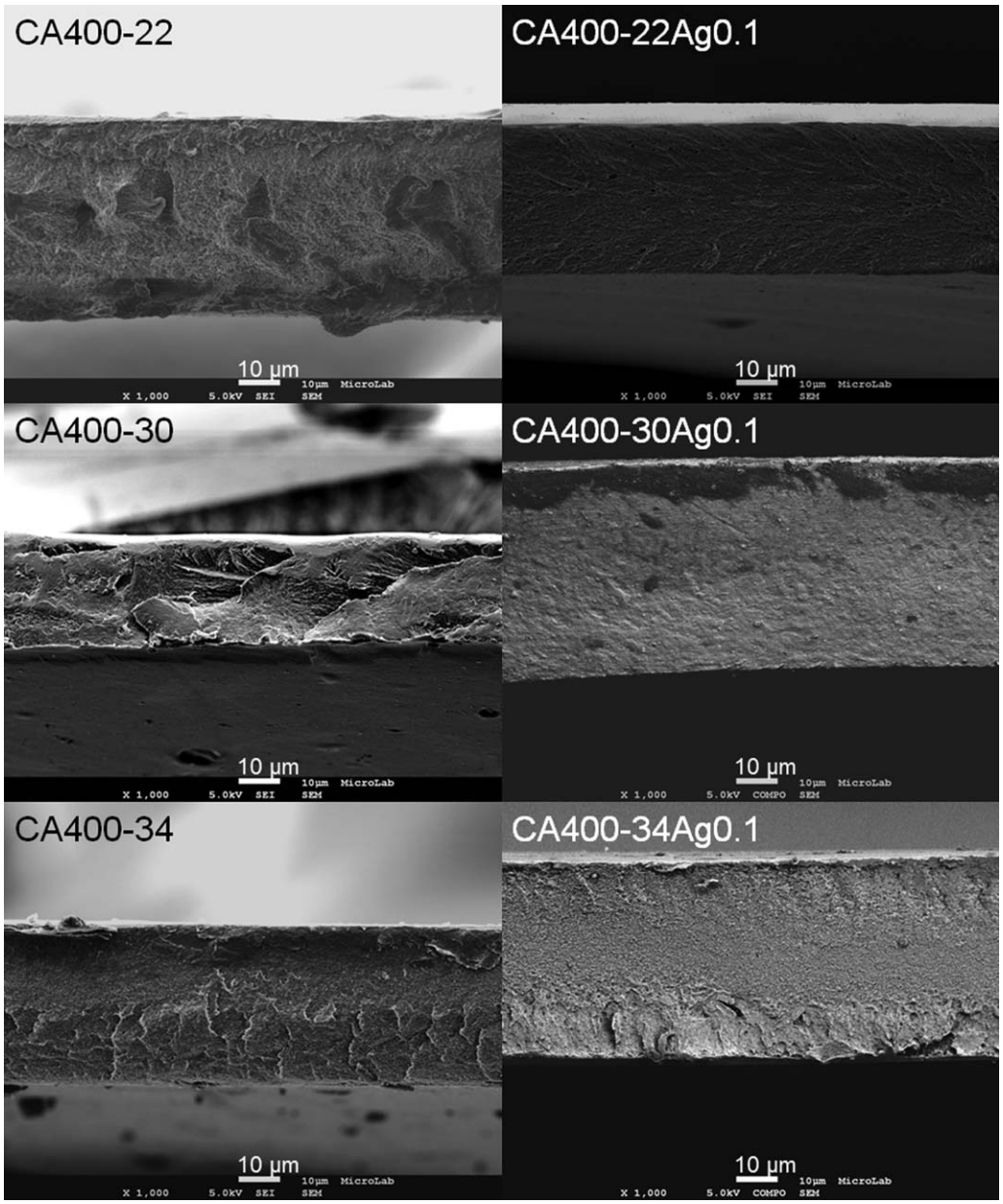

Figure 1. Cross-section views of CA400 membranes (left, pristine membranes, right, silver-containing membranes).

Table I shows the casting solutions composition and the casting conditions of the membranes prepared. For nanoparticle incorporation, the modified casting solution was prepared by the addition and mixing of the dispersion of Ag nanoparticles to the casting solution (Table I). The mixture was sonicated for 2 min. Special care was taken to ensure the homogeneous dispersion of the nanoparticles. An individual membrane is identified in Table I and throughout the text by a number whereby "22, 30, and 34" represent the wt % concentration of formamide considering the CA400 series free of silver (i.e., CA400-22, CA400-30, and CA400-34). For CA/silver nanocomposite membranes, the symbols "Ag0.1 and Ag0.4" represent the silver content of 0.1% wt and 0.4% wt, respectively (i.e., CA400-30Ag0.1 and CA400-30Ag0.4).

The incorporation of the Ag nanoparticles on the membranes was verified by FESEM using a JM-7001F FEG-SEM (JEOL) located at the IST (Lisbon). The morphology, size, and agglomeration degree of the particles were observed while they were embedded in the membrane. For FESEM characterization, the dry membrane samples were covered with gold before observation.

The microCT studies were performed using a compact desktop high-resolution Skyscan 1172 scanner (Brucker). This methodology is nondestructive (NDM), with the advantage that the samples do not require any kind of preparation or cutting, avoiding damages that could change their properties. The analytical setup consists of the combination of an object X-ray shadow digital images microscopic system and a computer with tomographic

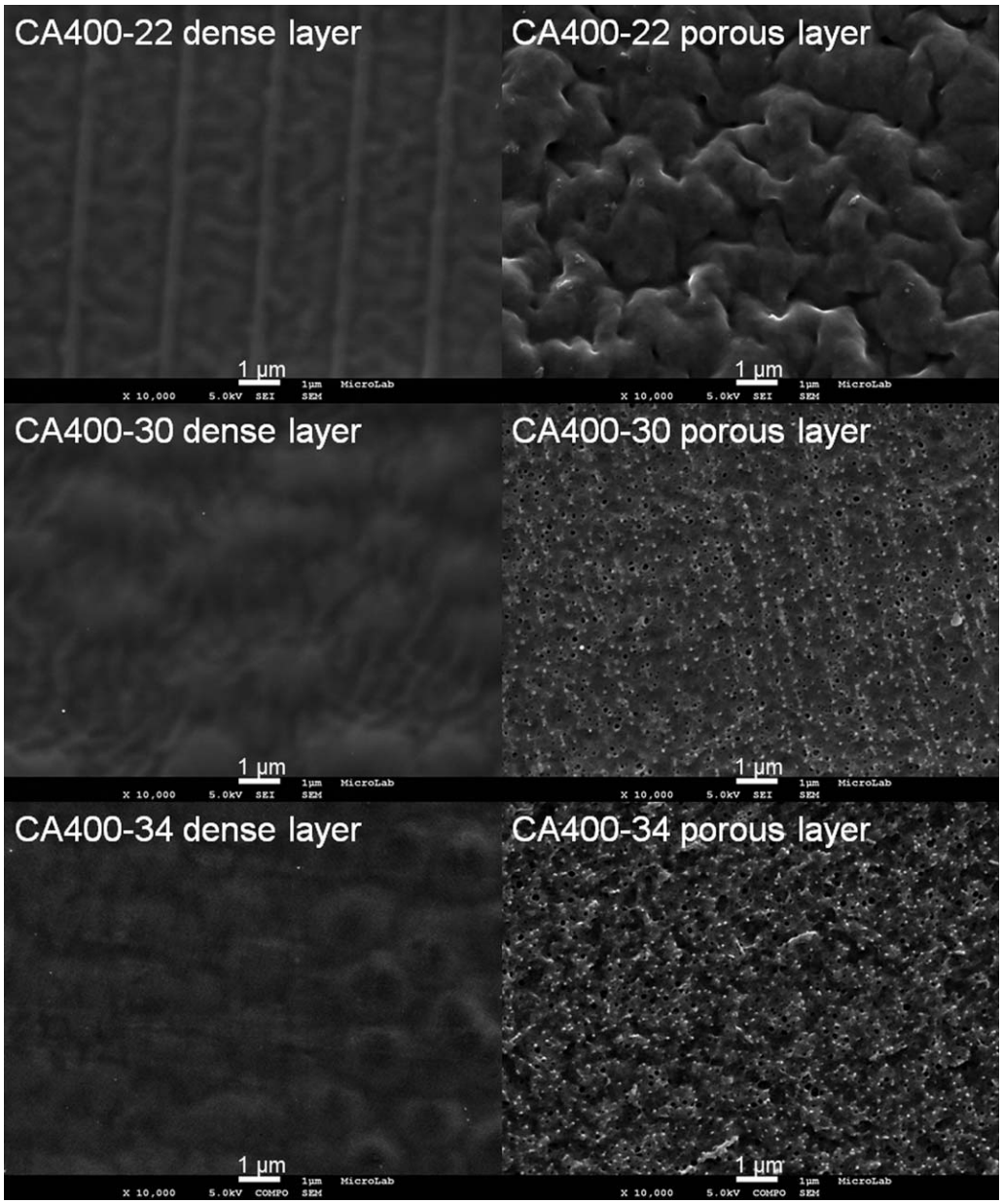

Figure 2. FESEM images of dense layer and porous layer of CA400 membranes, free of silver nanoparticles.

reconstruction and analysis software. X-ray source and detector are fixed, while the sample rotates around a stable vertical axis. Samples were scanned at a variable voltage (38–60 kV) and current intensity (240–167 μA) in order to enhance the phase contrast. The operation procedure was optimized to obtain the best images by reducing beam hardening, ring, star, and line artifacts as much as possible. Pixel size around 2–2.5 μm, close to the lower limit of the scanner, was chosen for the size scale of the membrane's components. A random movement of five with a five frame averaging was chosen to minimize noise. The basic physical parameter quantified in each pixel of a CT-image is the linear attenuation coefficient. Beer's law relates the intensity (I) of X-ray photons passing through the object with thickness h, with the incoming intensity (I_o) and the coefficient (μ (xyz)) at point (xyz) inside the object. In this study, the main variables affecting the beam attenuation are membrane average composition, structure (the size of the porous and/or incorporated silver particles), density, thickness, and compactness.

Permeation experiments were performed to characterize the membranes in terms of pure water hydraulic permeability (Lp), and molecular weight cut-off (MWCO). The permeation experiments were performed in a five flat plate cells with two detachable parts separated by a porous plate (membrane support), with a membrane surface area of 13.2×10^{-4} m^2 Before the experiments, the membranes were compacted for 2 h with deionized water at a transmembrane pressure of 3 bar. The hydraulic permeability is obtained by the slope of the straight line of pure water permeate fluxes (J_{pw}) as a function of the transmembrane pressure (ΔP) defined as $Lp = J_{pw}/\Delta P$. The range of the transmembrane pressure used was 1, 2, and 3 bar with a flow rate of 180 Lh^{-1}.

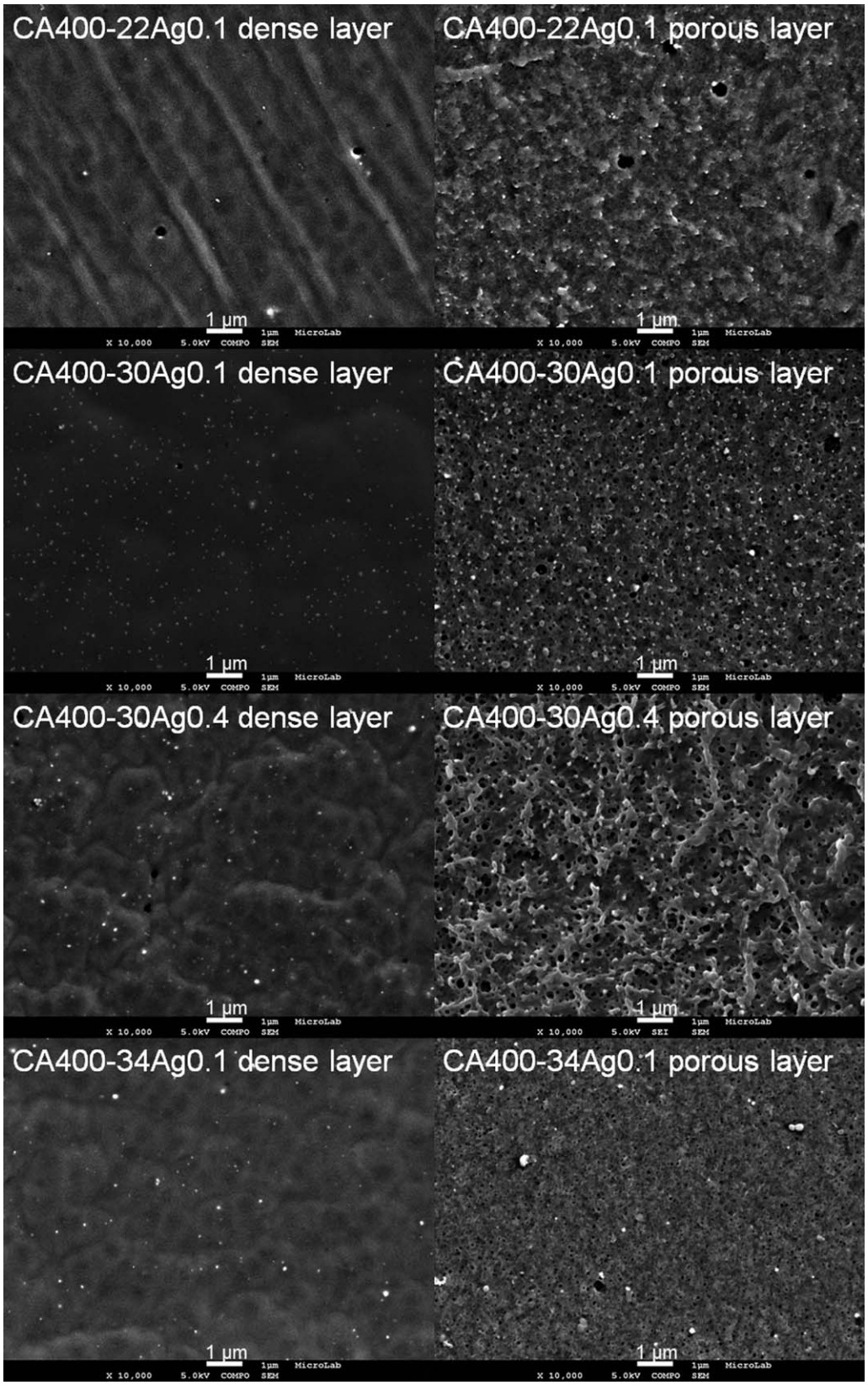

Figure 3. FESEM images of dense and porous layers of CA400 membranes containing silver nanoparticles (0.1 and 0.4% wt Ag).

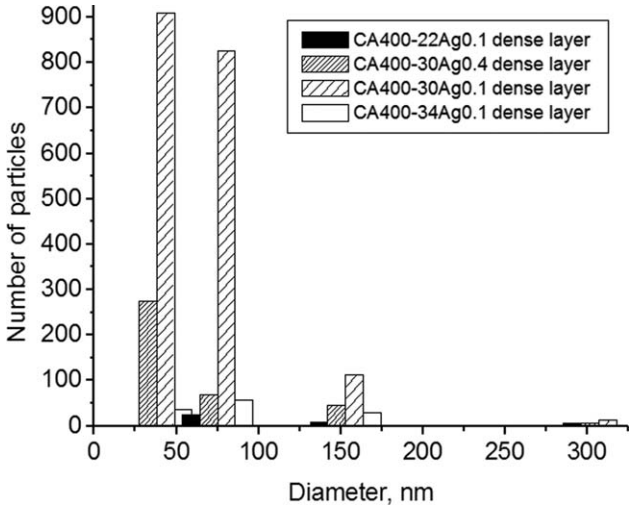

Figure 4. Total amount of silver nanoparticles in the images corresponding to the dense layers of silver-containing membranes of Figure 3, at magnification of 5000x.

The MWCO, parameter defined by the molecular weight of a determined macromolecule whose rejection is higher than 91%, was determined using the rejections of organic solutes, using several polyethylene glycol (PEG) and Dextran solutions. The apparent solute rejection coefficients (f) is defined as $f=(C_f-C_p)/C_f$, where C_f and Cp are the solute concentrations in the bulk of the feed solution and of the permeate solution, respectively. To determine the MWCO, the curve of $\log\left(\frac{f}{(1-f)}\right)$ as a function of the molecular weight of the organic solutes (PEG 1000, 3000, 6000, 10,000, 20,000, and 35,000 Da; Dextran 70,000 Da) was used. The MWCO value is obtained by the intersection of the straight line with the 91% rejection line, which correspond to a value of $\log\left(\frac{f}{(1-f)}\right)$ of 1.005. The stabilization time for each experimental run was 30 min. The organic solutes concentrations in feed and permeate solutions were determined in terms of total organic carbon (TOC) content, using a Dohrmann Total Organic Carbon Analyzer Model DC-85A.

In the experiments to assess the silver loss during the membrane storage and filtration, the membrane with the higher silver content, CA400-30Ag0.4, with a surface area of 13.2×10^{-4} m^2, was used. For the assessment of silver loss during storage, the membrane was immersed in 200 mL of distilled water for 218 days. To evaluate the loss of silver during filtration, pure water permeation experiments were carried out in the crossflow ultrafiltration unit at a feed flow rate of 180 Lh^{-1} and 3 bar. The silver concentration in the feed tank was also analyzed. The silver concentrations were determined by atomic absorption spectrometry at the LAIST laboratory.

Table II. Number of Silver Nanoparticles in the Images Corresponding to the Dense Layers of Silver-Containing Membranes of Figure 3 at Magnification of 5000×

Membrane	CA400-22Ag0.1	CA400-30Ag0.1	CA400-30Ag0.4	CA400-34Ag0.1
Number of particles	38	1863	399	124

RESULTS AND DISCUSSION

Figure 1 shows the micrographs of the cross-section views for membranes CA400 with and without silver. The cross sections of the silver-containing membranes display very uniform and smooth structures in contrast with the nonsmooth nature of the silver-free membranes.

The FESEM images (Figures 2 and 3) of the top and bottom surfaces of the membranes evidenced the asymmetric structure by the difference between them; that is, the pore size on the glass-contacting surface (porous layer) is larger than the one on the air-contacting surface (dense layer). In Figure 2, the dense layers and the porous layers of CA400 membranes (silver-free) are presented. The casting solution composition, namely the solvent/cosolvent ratio, greatly influences the membrane structure.[21,22] This is particularly noticeable in the porous layers, as the increase in formamide content and its effect on the cosolvent/nonsolvent transfer in the demixing process is well evidenced in the different structural features observed in the images. The image of the porous layer of the CA400-22 membrane displays a dense polymeric surface with very few pores. This is in clear contrast with the surface of the porous layers of the CA400-30 and CA400-34 membranes, which present many pores distributed throughout the all the surface. These membranes were casted from polymeric solutions with increasing formamide content (22%, 30%, and 34%, as shown in column 2, 4, and 7 of Table I, respectively). This is the only varying parameter, and it is crucial in the last step of casting where the amount of formamide exchanged with water (gelation medium) will determine the final porous structure of the membranes. Strathmann[22] reports that this effect of increase in the formamide content gets less pronounced and even in extent when the formamide content approaches 35%. In fact, the pore size and pore size distribution of the porous surfaces of the CA400-30 and CA400-34 membranes are very similar.

For membranes containing 0.1 and 0.4% wt silver (Figure 3) and using the backscattering electrons detector, the presence of "bright spots" in the surfaces of the dense layers is more visible than on the porous layer, giving evidence that there is an higher concentration of nanoparticles in the surface of this layer for membrane structures CA400-30 and CA400-34. This is due to the higher cellulose acetate polymer concentration at the dense layer, as a result of the wet-phase inversion evaporation step in terms of time and solvent volatility. Apparently, the particles remain at the dense layer and perhaps in close proximity to it, as the presence of particles on the porous layer is very scarce. The image corresponding to the dense layer of CA400-30Ag0.1 shows the adequate dispersion of silver in the membrane, giving a hint of the better compatibility of the dispersion containing the PVP-covered nanoparticles with the CA400-30 casting solution.

The micrograph corresponding to the porous layer of CA400-22Ag0.1 shows differences in structure when compared to its

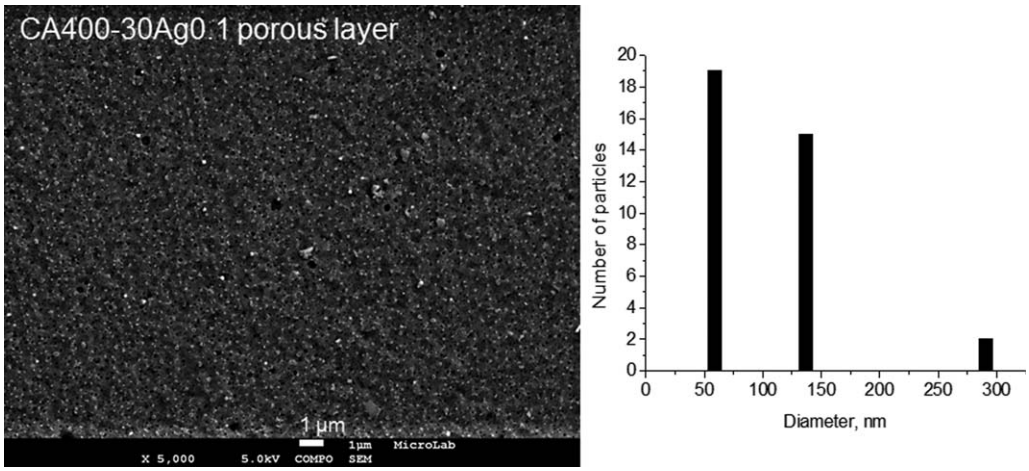

Figure 5. FEG-SEM micrograph of the bottom layer (porous layer) of membrane CA400-30Ag0.1, and size distribution of silver nanoparticles.

silver-free counterpart, giving some evidence of the pore-forming ability of the dispersion. It is worth mentioning that the stable dispersions of PVP-coated silver nanoparticles are prepared through aqueous solutions of PVP, and therefore, their addition to the casting solutions introduces not only PVP, but also water that can associate with formamide by hydrogen bonding, thus leading to the new casting solutions where the establishment of very different interactions between polymer/formamide/PVP-coated silver nanoparticles leads to membranes with very different characteristics. The influence of PVP and water is in itself another area of research.

The silver nanoparticles in the CA400-30Ag0.1 membrane are better distributed when compared to the distribution of the CA400-30Ag0.4 membrane. Apparently, the CA/acetone/formamide ratio 17 : 53 : 30 provides excellent chemical compatibility to the PVP-coated silver nanoparticles but to a certain extent. When the silver content is high, the particles agglomerate and the distribution is no longer homogeneous on the top layer of the membrane, and nevertheless, the particles remain in the nanometric range.

To confirm these assumptions, 5000x FESEM images of the top and of the porous layers were analyzed using the software CTAN, in order to get more information about particles and pore sizes, as well as their distribution density. Figure 4 shows the size histogram obtained for the dense layer of the membranes containing silver. The greatest amount of particles (Table II) was found for membrane CA400-30Ag0.1, and most of the particles were smaller than 76 nm.

Size analysis of silver nanoparticles for the porous layer was carried out only for membrane CA400-30Ag0.1 (Figure 5), as the amount of silver in the other membranes was negligible. The size analysis shows (even though the amount of particles analyzed is low) that the Ag particles located in the porous layer of the membrane "CA400-30Ag0.1" are bigger than the fine particles located in the top layer ("CA400-30Ag0.1 dense layer," Figure 3). From Figure 5, the particles are apparently more loosely bounded to the polymeric phase, and it is possible that these particles are lost at the first stages of permeation. Experiments to confirm this assumption will be carried out in a future work.

The same procedure was made for the pores analysis of the bottom surface of the porous layers, and the results are presented in Figure 6. No pores are visible on the top layers as they have diameters below the technique detection limit of several nanometers.

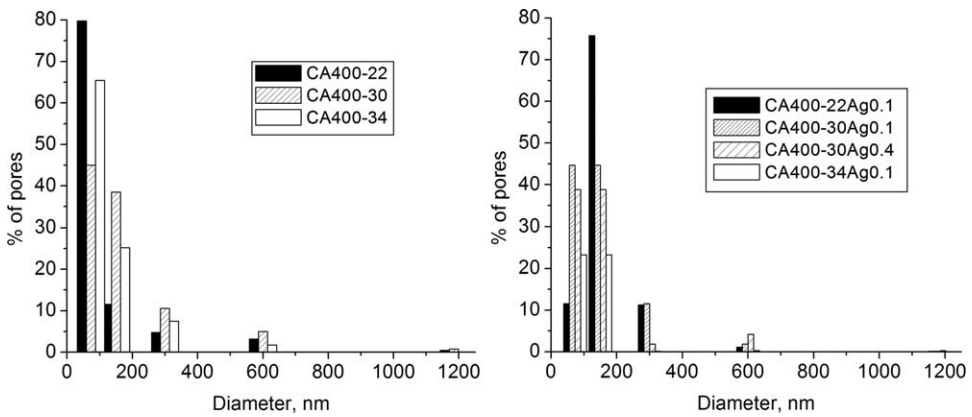

Figure 6. Pore size and percentage and size of pores in the images corresponding to membranes at 5000x.

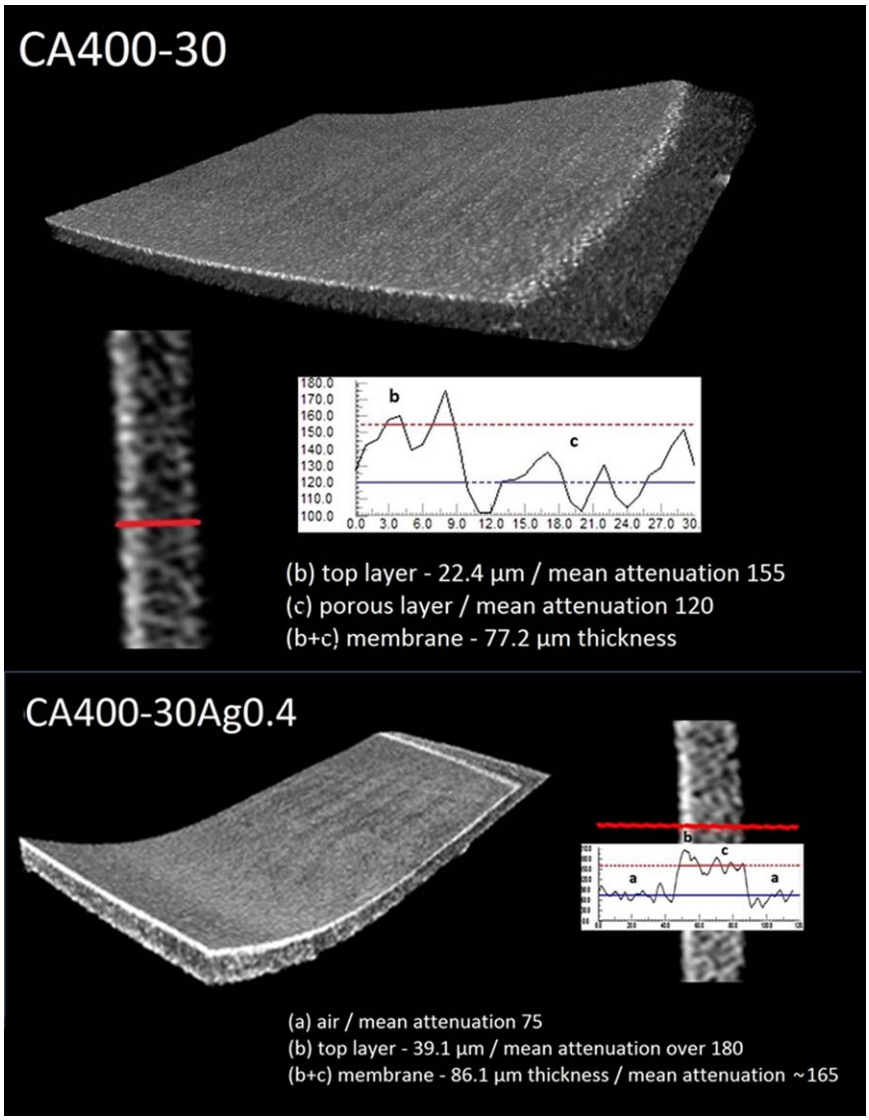

Figure 7. Three-dimensional models of the membranes CA400-30 (2.49 pixel size) and CA400-30Ag0.4 (1.96 pixel size). Cross-section (red line) attenuation profiles showing asymmetrical structure of the membranes with a more compact top layer. Higher values of attenuation in the CA400-30Ag0.4 membrane are related to the presence of the silver particles. [Color figure can be viewed in the online issue, which is available at wileyonlinelibrary.com.]

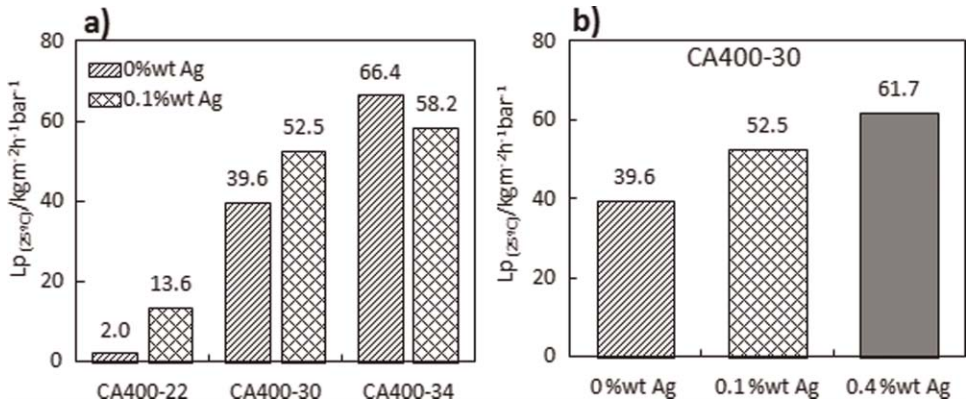

Figure 8. (a) Hydraulic permeabilities results for membranes prepared from casting solutions with different acetone/formamide ratios (CA400-22, CA400-30, CA400-34), with 0% wt Ag and 0.1% wt Ag. (b) Hydraulic permeabilities results for membranes obtained through casting solution with the same acetone/formamide ratio (CA400-30) and different silver contents (0% wt Ag, 0.1% wt Ag, 0.4% wt Ag).

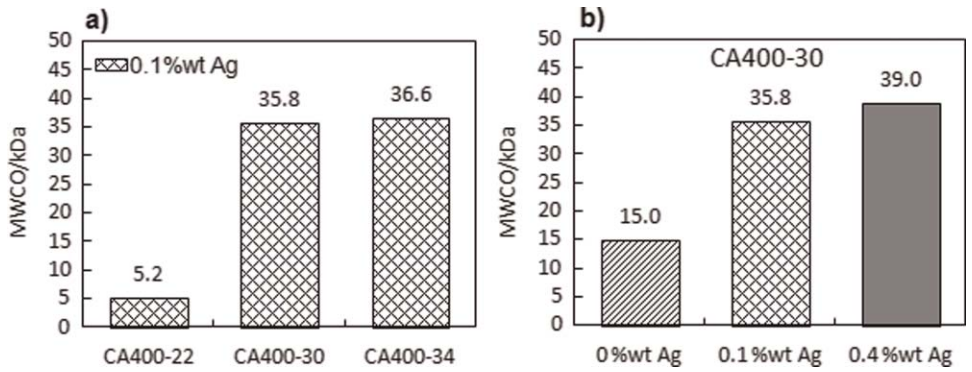

Figure 9. (a) MWCO results for membranes prepared from casting solutions with 0.1% wt Ag and different acetone/formamide ratios (CA400-22, CA400-30, CA400-34). (b) MWCO results for membranes obtained from casting solutions with the same acetone/formamide ratio (CA400-30) and different silver content (0% wt Ag, 0.1% wt Ag, 0.4% wt Ag).

The pore-forming ability of the PVP-covered silver particles is not evident except for the composition CA-400-34 if only the pores quantity is considered, and, on the other hand, this size analysis confirmed the importance of the casting solution composition on porosity. Another observation is the fact, that the addition of the dispersion might not influence the number of pores to a significant extent (except for CA400-34 membranes as already mentioned), but for CA400-22 and CA400-30 membranes, it promotes the formation of bigger pores. The amount of dispersion added seems to have the same effect for membranes of the type CA400-30, but the amount of pores drastically diminishes when the PVP-covered silver increases.

Figure 7 shows 3D models of the membranes CA400-30 and CA400-30Ag0.4 obtained by using the CTVox program. As mentioned in the experimental part, this methodology is nondestructive, with the advantage that the samples do not require any kind of preparation or cutting, avoiding damages that could change their properties. One example of damage is shown in the Figure 1, where an apparent macroporosity is observed. The CA400-30 membrane surface exposed at 1000x magnification is related to the cutting of the sample. Therefore, this is a methodology that provides 3D information and can be used at an early stage of the study to define strategies for subsequent techniques of characterization. The results enable us to distinguish the main structural differences between pristine- and Ag-bearing membranes. Both membranes show a more compact top layer (b), corresponding to a higher value of X-ray attenuation (brighter pixels). The attenuation contrast between the top layer (b) and the inner part of the membranes (c) is clearly visible in both cases. But in the CA400-30Ag0.4 membrane the high value of attenuation is due the presence of Ag nanoparticles. These differences could be seen in more detail in the selected attenuation profiles. The porous layer's structures present a bumpy aspect, corresponding to the mixing of cellulose acetate and submicroscopic pores, which is in accordance with SEM observations (Figures 1 and 2).

It is likely that parts of the features present in the membranes are under the spatial resolution of the laboratory desktop microscanner used in this study. To this assessment, further tomographical studies at nanometer pixel size scales are necessary to obtain more precise and accurate 3D models of the different layers, and a desktop nanoscanner or synchrotron radiation must be applied. In this way, an extended characterization of the membranes structure can be made, namely their pore size distribution and connectivity, enabling these models to provide, after their statistical validation, useful information relative to membranes permeability and other structural studies.

Figures 8 and 9 summarize the permeation results in terms of hydraulic permeability and molecular weight cut-off. For these experiments, silver-free (CA400-22; CA400-30; CA400-34) and silver-containing (CA400-22Ag0.1; CA400-30Ag0.1; CA400-34Ag0.1) membranes from different casting solutions were used. Besides, for the CA400-30, two other membranes with different nanoparticles contents (0% wt and 0.4% wt) were also tested. Figure 8a presents the results for hydraulic permeability for membranes CA400-22, CA400-30, and CA400-34 without silver nanoparticles and with 0.1% wt silver content. Comparing the hydraulic permeabilities for membranes obtained from casting solutions CA400-22 and CA400-30, without and with 0.1% Ag nanoparticles, is particularly evident an enhancement of permeability for the membranes containing silver. With respect to the less dense membranes prepared from a casting solution with a higher content in formamide (CA400-34), this enhancement by

Table III. Number of Pores in the Images Corresponding to the Membranes at 5000×

Membrane	CA400-22	CA400-22Ag0.1	CA400-30	CA400-30Ag0.1	CA400-30Ag0.4	CA400-34	CA400-34Ag0.1
Number of pores	3270	3362	8201	7805	4617	8372	11439

the introduction of silver nanoparticles is not observed and even presented a small decrease in the hydraulic permeability value. Although the effect of PVP during membrane preparation remains unclear, and nanoparticle-induced changes in the membrane structure depends to a great extent of the particle/polymer combination, some trends can be identified. As Strathmann[22] reports, the effect of increase in the formamide content gets less pronounced and even nonexistent when the formamide content approaches 35%. The nanoparticle-induced changes on the membrane structures are also observed only for the less porous membranes. According to Taurozzi *et al.*, the introduction of silver nanoparticles into a polyetherethersulfone matrix induced noticeable changes in morphological properties and permeate flux only in membranes with a denser structure.[23]

In Figure 8b, the influence of different silver nanoparticles contents (0, 0.1, and 0.4% wt Ag) in the hydraulic permeabilities are represented, for membranes obtained from casting solutions with the same acetone/formamide ratio (CA400-30). With the incorporation of 0.1 and 0.4% wt Ag of silver nanoparticles, we observed an increase in around 33% and 56%, respectively. The addition of 0.1% wt Ag in the CA400-30 casting solution introduced an increase in the hydraulic permeability from 39.6 to 52.5 $kgm^{-2}h^{-1}bar^{-1}$, and the increment from 0.1 to 0.4% wt Ag results in an increase from 52.5 to 61.7 $kgm^{-2}h^{-1}bar^{-1}$. This is a curious fact since the results in Figure 6 and Table III show a decrease in the number of pores with increasing silver content, but in general with an increase in the pores size. Chou *et al.*,[7] in their experiments of loading silver in cellulose acetate hollow fiber membranes, also obtained a higher value of hydraulic permeability for the membranes with silver, and they obtained an increase in 10% for the addition of silver between 0.001–0.1% wt of $AgNO_3$.

The influence on MWCO of the use of different acetone/formamide ratios in the casting solution, of membranes containing 0.1% wt Ag, is presented (Figure 9a). The results show a significant increase in the MWCO when the ratio of acetone/formamide goes from 2.77 (CA400-22) to 1.76 (CA400-30), but this increase is not so high when the values obtained for the membranes obtained from a casting solution with an acetone/formamide ratio of 1.76 (CA400-30) and 1.44 (CA400-34) are compared.

The influence on the MWCO of increasing the silver nanoparticles content in membranes prepared from the casting solution with acetone/formamide ratio of 1.76 (CA400-30) is reported in Figure 9b. These results show a substantial increase in the membrane MWCO with the addition of 0.1% wt Ag (35.8 kDa) when compared with the silver-free membrane (15 kDa). If the Ag content increases from 0.1 to 0.4% wt Ag in membrane CA400-30 causes, the increase in the MWCO is not so considerable (from 35.8 to 39.0 kDa).

From the results, it is observed that with the addition of 0.1% wt Ag to the CA400-30 casting solution, a more significant increase (33%) in the hydraulic permeabilities was obtained than when the silver nanoparticles content was increased from 0.1 to 0.4% wt Ag, where an increase in 18% was observed. And, regarding to the MWCO, a similar behavior is noted, the introduction of 0.1% wt Ag in the casting solution results in an increase in 139% and the increase from 0.1 to 0.4% wt Ag leads to an increment of only 9% when related with the addition of 0.1% wt Ag. An increase in permeation flux of the membrane can be attributed to a hydrophilicity increase due to the presence of nanoparticles.

The experiments developed to assess the silver loss in a CA400-30Ag0.4 membrane during water filtration revealed a result of 5.9 ppb for permeate. The silver concentration in the feed tank was also analyzed presenting values in the range of 1 ppb in silver, very close to the lower limit detection of the equipment. World Health Organization (WHO) states that the value of 100 ppb for silver as tolerant for drinking water without risk to human health, and the level of silver obtained in the permeate (5.9 ppb) is about two orders of magnitude lower than this value.[24]

CONCLUSIONS

In this work, the effects of casting solution composition and nanoparticles incorporation in the morphological and separation properties of porous nanocomposite membranes were studied, using PVP-covered silver, added as an aqueous dispersion, as the filler material. In this method of incorporation, it was demonstrated that concentrated solution of silver nanoparticles, with control of nonagglomeration in the casting formulations, results in markedly different nanocomposite morphologies. The casting solution composition yields differences in membrane structure and Ag distribution on both surfaces of the matrix, showing the influence of the affinity of the filler material for the components of casting mixture. It was evidenced that nanocomposite membranes present a higher silver nanoparticles concentration in the dense layer, with a better distribution to the membrane with lower silver content, and FESEM images illustrate evidences of the absence of nanoparticles agglomerations. In some membranes, silver incorporation induced a significant increases in the hydraulic permeability and molecular weight cut-off, and in permeation conditions, a very low silver loss to the permeate was observed. These results allow us to develop further studies in terms of bactericide properties of these nanocomposite membranes.

ACKNOWLEDGMENTS

M.G.S.L., on sabbatical leave from the UASLP at IST, acknowledges CYTED for the partial financial support. A.S.F. enjoys a half-time teaching leave from the ISEL/IPL to develop doctoral work at IST. We also thank M.Sc. Isabel Nogueira, IST/ICEMS/Microlab for SEM characterization.

REFERENCES

1. Arthanareeswaran, G.; Thanikaivelan, P. *Sep. Purif. Technol.* **2010**, *74*, 230.
2. Sawada, I.; Fachrul, R.; Ito, T.; Ohmukai, Y.; Maruyama, T.; Matsuyama, H. *J. Membr. Sci.* **2012**, *387*, 1.
3. Li, J. H.; Shao, X. S.; Zhou, Q.; Li, M. Z.; Zhang, Q. Q. *Appl. Surf. Sci.* **2013**, *265*, 663.

4. Bergamasco, R.; da Silva, F. V.; Arakawa, F. S.; Yamaguchi, N. U.; Reis, M. H. M.; Tavares, C. J.; de Amorim, M. T. P. S.; Tavares, C. R. G. *Chem. Eng. J.* **2011**, *174*, 102.
5. Yu, D. G.; Teng, M. Y.; Chou, W. L.; Yang, M. C. *J. Membr. Sci.* **2003**, *225*, 115.
6. Son, W. K.; Youk, J. H.; Lee, T. S.; Park, W. H. *Macromol. Rapid Commun.* **2004**, *25*, 1632.
7. Chou, W. L.; Yu, D. G.; Yang, M. C. *Polym. Adv. Technol.* **2005**, *16*, 600.
8. Sotto, A.; Boromand, A.; Zhang, R.; Luis, P.; Arsuaga, J. M.; Kim, J.; Van der Bruggen, B. *J. Colloid Interface Sci.* **2011**, *363*, 540.
9. Balta, S.; Sotto, A.; Luis, P.; Benea, L.; Van der Bruggen, B.; Kim, J. *J. Membr. Sci.* **2012**, *389*, 155.
10. Perreault, F.; Tousley, M. E.; Elimelech, M. *Environ. Sci. Technol. Lett.* **2014**, *1*, 71.
11. Pendergast, M. M.; Hoek, E. M. V. *Energy Environ. Sci.* **2011**, *4*, 1946.
12. Murphy, D.; de Pinho, M. N. *J. Membr. Sci.* **1995**, *106*, 245.
13. Dias, C. R.; Rosa, M. J.; de Pinho, M. N. *J. Membr. Sci.* **1998**, *138*, 259.
14. Dias, C. R.; de Pinho, M. N. *J. Mol. Liq.* **1999**, *80*, 117.
15. Stamatialis, D. F.; Dias, C. R.; de Pinho, M. N. *Biomacromolecules* **2000**, *1*, 564.
16. Abedini, R.; Mousavi, M. S.; Aminzadeh, R. *Chem. Ind. Chem. Eng. Q.* **2012**, *18*, 385.
17. Hachisuka, H.; Ohara, T.; Ikeda, K. *J. Membr. Sci.* **1996**, *116*, 265.
18. Tashdjian, A.; Sánchez-Loredo, M. G.; González, G. A. *Electroanalysis* **2013**, *25*, 2124.
19. Desai, R.; Mankad, V.; Gupta, S. K.; Jha, P. K. *Nanosci. Nanotechnol. Let.* **2012**, *4*, 30.
20. Kunst, B.; Sourirajan, S. *J. Appl. Polym. Sci.* **1974**, *18*, 3423.
21. Kesting, R. "Synthetic Polymeric Membranes. A Structural Perspective," John Wiley and Son, **1985**, p 186, 237.
22. Strathmann, H. "Synthetic Membranes and Their Preparation." Bungay, P. M.; Lonsdale, H. K.; Pinho, M. N. Eds. "Synthetic Membranes: Science, Engineering and Applications," NATO ASI Series, D. Reidel Publishing Company, **1986**, 1.
23. Taurozzi, J. S.; Arul, H.; Bosak, V. Z.; Burban, A. F.; Voice, T. C.; Bruening, M. L.; Tarabar, V. V. *J. Membr. Sci.* **2008**, *325*, 58.
24. WHO-World Health Organization. Guidelines for Drinking Water Quality. Geneva, Switzerland, **2003**.